

# Precession of the Sagittarius stream

V. Belokurov<sup>1\*</sup>, S. E. Koposov<sup>1,2</sup>, N.W. Evans<sup>1</sup>, J. Peñarrubia<sup>1,3</sup>, M.J. Irwin<sup>1</sup>, M.C. Smith<sup>4</sup>, G.F. Lewis<sup>1,5</sup>, M. Gieles<sup>1,6</sup>, M. Wilkinson<sup>7</sup>, G. Gilmore<sup>1</sup>, E. W. Olszewski<sup>8</sup>, and M. Niederste-Ostholt<sup>1</sup>

<sup>1</sup>*Institute of Astronomy, Madingley Rd, Cambridge, CB3 0HA,*

<sup>2</sup>*Sternberg Astronomical Institute, Moscow State University, Universitetskii pr. 13, Moscow 119991, Russia*

<sup>3</sup>*Institute for Astronomy, Royal Observatory, Blackford Hill View Edinburgh, City of Edinburgh EH9 3HJ*

<sup>4</sup>*Shanghai Astronomical Observatory, 80 Nandan Road, Shanghai 200030, China*

<sup>5</sup>*Sydney Institute for Astronomy, School of Physics, A28, The University of Sydney, NSW 2006, Australia*

<sup>6</sup>*Department of Physics, University of Surrey, Guildford, GU2 7XH, UK*

<sup>7</sup>*Department of Physics & Astronomy, University of Leicester, Leicester LE1 7RH*

<sup>8</sup>*Steward Observatory, University of Arizona, Tucson, AZ 85721, USA*

December 2012

## ABSTRACT

Using a variety of stellar tracers – blue horizontal branch stars, main-sequence turn-off stars and red giants – we follow the path of the Sagittarius (Sgr) stream across the sky in Sloan Digital Sky Survey data. Our study presents new Sgr debris detections, accurate distances and line-of-sight velocities that together help to shed new light on the puzzle of the Sgr tails. For both the leading and the trailing tail, we trace the points of their maximal extent, or apo-centric distances, and find that they lie at  $R^L = 47.8 \pm 0.5$  kpc and  $R^T = 102.5 \pm 2.5$  kpc respectively. The angular difference between the apo-centres is  $93.2 \pm 3.5^\circ$ , which is smaller than predicted for isothermal haloes. It is consistent with models of the Milky Way in which the dark matter density falls more quickly with radius. Based on its position and radial velocity, we show that the unusually large globular cluster NGC 2419 is associated with the Sgr trailing stream. We measure the precession of the orbital plane of the Sgr debris in the Milky Way potential and show Sgr debris in the primary tails evolves differently to the secondary tails, both in the North and the South.

**Key words:** Galaxy: fundamental parameters — Galaxy: halo — Galaxy: kinematics and dynamics — stars: blue stragglers — stars: carbon — stars: horizontal branch

## 1 INTRODUCTION

As long as Newton’s law of attraction holds true, an orbit gives the most straightforward method of inferring the underlying gravitational potential. Such an inference is truly unambiguous when the orbit mapped is nearly complete, as demonstrated beautifully by the recent measurements of the mass of the Milky Way’s central black hole (e.g. Ghez et al. 2008). At larger Galactocentric distances, orbital periods quickly grow to a significant fraction of the Hubble time, rendering the tracking of a trajectory impractical. Yet, it is still possible to establish the paths of some infalling Galactic fragments rather accurately even at distances beyond many tens of kpc. Certain Milky Way satellites sprout stellar tidal tails long enough to delineate some of their orbit. These include the Sagittarius dSph stream (Majewski et al. 2003), the tails of the Palomar 5 globular cluster (Odenkirchen et al. 2003), as well as the Orphan

(Belokurov et al. 2007) and the GD-1 (Grillmair & Dionatos 2006) streams.

So far, the most robust inference of the Galactic potential based on the measurements of a stellar stream has been the one carried out with the GD-1 system by Koposov et al. (2010). Even though only  $\sim 100^\circ$  of arc of the stream has been mapped, the detailed phase-space information and the intrinsic coldness of the stellar debris allowed the authors to avoid the degeneracies inherent in the stream modelling process (e.g. Eyre & Binney 2009). However, given the orbit of the GD-1 stream, the circular velocity measurement it facilitates, while independent and robust, is limited to the range of galactocentric distances accessible to other techniques (e.g. Bovy et al. 2012).

To reach into the outer Galactic halo, more distant and luminous streams like the Orphan or Sagittarius are needed. The kinematically cold Orphan stream seems to possess the properties ideal for orbit inference. However, compared to the total of only  $\sim 60^\circ$  of the available detections of the Orphan Stream at distances between 30 and 50 kpc, there exists much more abundant information for both the leading and the trailing tail of the Sgr stream.

\* E-mail: vasily@ast.cam.ac.uk

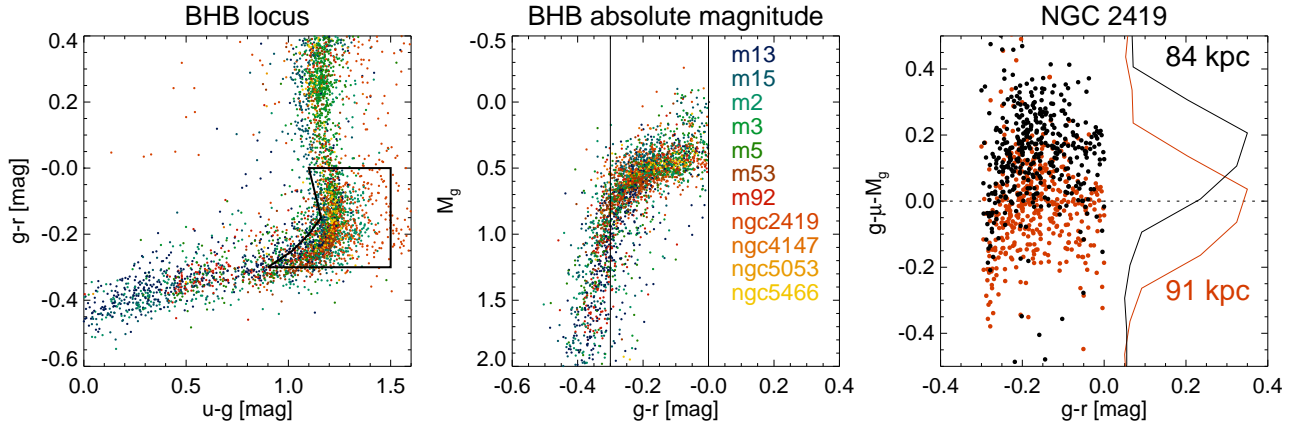


**Figure 1.** BHB stars in SDSS bands. *Left:* BHB  $u-g$ ,  $g-r$  locus as traced by the BHB stars in the Galactic star clusters. Each dot represents a BHB candidate star coloured according to the membership in one of the 11 clusters listed in the middle panel. The polygon shows the region proposed by Yanny et al. (2000) to select BHBs. *Middle:* BHB absolute magnitude as a function of  $g-r$  colour. Note how stars belonging to different star clusters group densely around similar intrinsic luminosity which changes slowly with  $g-r$  colour. Vertical black lines mark the boundaries of the selection region shown in the Left panel. *Right:* Offset between the distance modulus calculated using eq. 7 of Deason et al. (2011) and the distance modulus suggested by Harris (1996) for the BHB candidate stars in the globular cluster NGC 2419. Red dots are for the assumed heliocentric distance to NGC 2419 of 91 kpc. Curves show the histograms of the distance modulus offset.

Each extends some  $\sim 180^\circ$  of arc, probing Galactocentric distances in the range of 20-100 kpc. As of today, the narrow, but relatively faint Orphan stream remains largely unstudied, yet a broad-brush picture of the wide and luminous Sgr stream is slowly taking shape, thanks to the diversity of the disruption models at hand (e.g. Ibata et al. 2001; Helmi 2004; Johnston et al. 2005; Fellhauer et al. 2006; Law & Majewski 2010; Peñarrubia et al. 2010).

The most comprehensive model to date (Law & Majewski 2010) fits accurately the 3D positions and the radial velocities of the brightest components of the leading and the trailing tail as mapped by Belokurov et al. (2006); Law et al. (2004), and Majewski et al. (2003, 2004) respectively. This N-body simulation, however, does not provide an explanation for the tail “bifurcations” observed both in the North and the South (Belokurov et al. 2006; Koposov et al. 2012). Furthermore, the model does not produce Sgr tidal debris running with the opposite distance gradient at the locations of the leading tail around the North Galactic Cap (Branch C in the notation of Belokurov et al. (2006)), or the distant debris as detected by Newberg et al. (2003) in the direction of the Galactic anti-centre. Naturally, given the wealth of the data available for the Sgr system and the inherent complexity of the Milky Way’s gravitational potential, it is prudent to adopt the modelling strategy in which some of the many unknowns are fixed at their best-guess values. For their experiment, Law & Majewski (2010) chose to fix most of the orbital properties of the Sgr progenitor, as well as many of the ingredients describing the Galactic potential. For example, the potential of the dark matter halo is set to be logarithmic, while the importance of changing the shape of the dark halo is explored.

In this Paper, based on the Sloan Digital Sky Survey Data Release 8 (SDSS DR8) we i) present several new detections of the Sgr debris in the Galactic North, ii) refine some of the stream distances and iii) substantiate the 3D data with the measurements of the stream’s radial velocity. As a result, we show that the Branch C (Belokurov et al. 2006) and the anti-centre debris (Newberg et al. 2003) are all part of the very long trailing tail of the Sagittarius dwarf. We show that at the very edges of the SDSS footprint, both the leading and trailing tail reach their respective apo-centres, thus indicating that the galactocentric orbital precession (or apsidal pre-

cession) of the Sgr dSph is close to  $\sim 95^\circ$ . This is to be compared with logarithmic haloes, where the orbital precession is typically  $\sim 120^\circ$ . The lower rate of the orbital precession signifies a sharper drop in the dark matter density as a function of Galactocentric radius. We also measure the precession of the plane of the Sgr debris. This is related to the Sgr orbital plane evolution under the torques from the disk and the dark halo of the Milky Way.

## 2 STREAM TOMOGRAPHY WITH MULTIPLE TRACERS

For all the subsequent analysis, we correct the SDSS photometry for the effects of extinction using the dust maps of Schlegel et al. (1998). To correct for the solar reflex motion, we adopt  $V_{\text{LSR}} = 235$  km/s and  $(U, V, W) = (11.1, 12.2, 7.25)$  (Schönrich et al. 2010).

### 2.1 Blue Horizontal Branch stars in SDSS and the distance to NGC 2419

To measure mean heliocentric distances to portions of the Sgr stream within the SDSS field of view, we use Blue Horizontal Branch (BHB) stars. The luminosity of BHBs does not vary to any significant degree with changing age and metallicity and is primarily a function of the star’s temperature, which makes them attractive standard candles. Yanny et al. (2000) have shown that using the SDSS  $u-g$  and  $g-r$  colours, highly complete (for a particular range of effective temperatures) samples of BHBs can be selected with low levels of contamination. At high Galactic latitudes, the principal source of false positives within the boundaries of the colour-colour box proposed by Yanny et al. (2000) are the intrinsically less luminous Blue Straggler (BS) stars.

Figure 1 shows the properties of the candidate BHB stars in 11 Galactic star clusters analysed by An et al. (2008). The left panel of the Figure confirms the effectiveness of the colour cuts suggested by Yanny et al. (2000). BHBs from clusters with different stellar

populations essentially lie on top of each other forming a tight locus going bluewards in  $g - r$  at constant  $u - g$  and eventually turning blue in  $u - g$  at around  $g - r \sim -0.35$ . As is obvious from the middle panel of this Figure, the absolute magnitude of a BHB varies with its  $g - r$  color, as governed by changing temperature. At small negative values of  $g - r$ ,  $M_g \sim 0.5$ . However, on moving bluewards, the Horizontal Branch tips and by  $g - r = -0.35$ , the absolute magnitude is at least half a magnitude fainter. The behaviour of the centroid of the distribution of the Galactic globular cluster BHBs in the plane of absolute magnitude and  $g - r$  colour can be described accurately with a 4th degree polynomial, as proposed by Deason et al. (2011). In what follows, we use Equation 7 from Deason et al. (2011) to assign distances to candidate BHB stars within the colour-colour box outlined in the Left panel of Figure 1.

Only one globular cluster has significant non-zero residuals when the distance modulus  $(m - M)_g$  calculated using the BHB distance calibration described above is compared with  $(m - M)_g$  found in the literature. This is illustrated in the right panel of Figure 1. As apparent from the histograms of the  $(m - M)_g$  residuals in the right hand side of the panel, the distance modulus for NGC 2419 needs to be revised  $\sim 0.2$  mag upwards, thus making its heliocentric distance not 84 kpc (Harris 1996), but 91 kpc. Recently, Fermani & Schönrich (2013) presented new calibration of the BHB absolute magnitude based on theoretical isochrones. Compared to Deason et al. (2011) these models predict slightly higher ( $\sim 0.1$  mag) luminosity for stars as metal-poor as those in NGC 2419. To test whether some of the 0.2 mag discrepancy observed here could be explained away by this effect, we checked the  $(m - M)_g$  residuals for three more star clusters with  $[\text{Fe}/\text{H}] < -2$ , namely M 92, M15 and NGC 5053. The residuals for the stars in all three clusters stay firmly on zero. While our slightly higher distance estimate is mildly inconsistent with the value provided by Harris (1996), we are in agreement with the most recent RR Lyrae measurement by Di Criscienzo et al. (2011).

## 2.2 The Sgr Stream signal in the SDSS data

Majewski et al. (2003) and Koposov et al. (2010) have shown that measuring the properties of a stellar stream can be highly robust (even with small numbers of stream members) if the debris mapping is performed in a coordinate system aligned with the stream. We follow the prescription of Majewski et al. (2003) and transform equatorial RA and Dec into a heliocentric  $\Lambda_\odot, B_\odot$  coordinate system whose equator is aligned with the Sgr trailing tail. Note, however, that in this paper  $\Lambda_\odot$  increases in the direction of Sgr motion, opposite to the convention used by Majewski et al. (2003).

The top panel of Figure 2 shows the density of (primarily) MSTO stars selected using the colour-magnitude cuts identical to those in Koposov et al. (2012). Both “branches” of the Sgr leading tail are visible superposed onto the Virgo overdensity at  $70^\circ < \Lambda_\odot < 120^\circ$ . Also visible are the Orphan stream at  $130^\circ < \Lambda_\odot < 150^\circ$  and the Monoceros ring at  $\Lambda_\odot \sim 170^\circ$ . The only tentative evidence of the presence of the trailing tail in the Northern SDSS data is the faint overdensity running between the Branches A and B at  $150^\circ < \Lambda_\odot < 160^\circ$  at constant  $B_\odot \sim -5^\circ$ . Note that even though the contiguous coverage of the main SDSS footprint runs out at  $\Lambda_\odot \sim 70^\circ$  and  $\Lambda_\odot \sim 170^\circ$ , within  $|B_\odot| < 10^\circ$  there exist several stripes reaching as far out as  $\Lambda_\odot \sim 40^\circ$  and  $\Lambda_\odot \sim 190^\circ$ , providing an additional  $\sim 50^\circ$  along the stream.

Indeed, the stream is clearly visible at both lower and higher  $\Lambda_\odot$ , as revealed by the density of the candidate BHB stars in

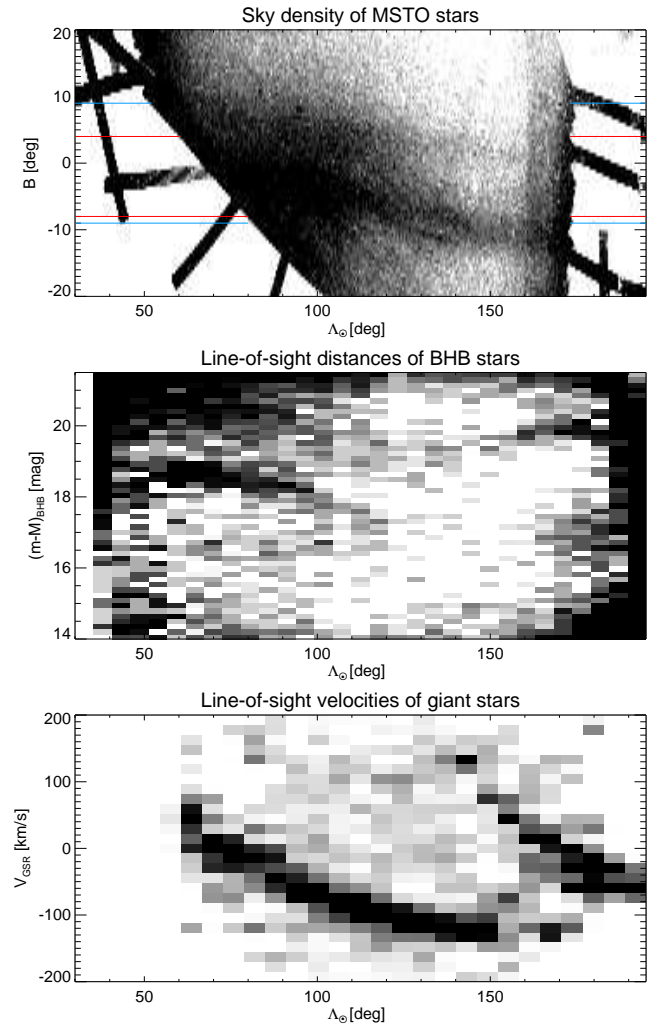


**Figure 2.** Sagittarius stream tomography with multiple tracers. Darker regions correspond to enhanced stellar density. *Top:* Sky density of MSTO stars in the Sgr stream coordinate system as defined by Majewski et al. (2003). Red (blue) lines show the range of latitude  $B$  used to select stars for Middle (Bottom) panel. *Middle:* Density of stream stars in the plane of Sgr stream longitude  $\Lambda_\odot$  and distance modulus. For this plot, BHB candidate stars with  $-8^\circ < B < 4^\circ$  are selected using the criteria of Yanny et al. (2000), while the distances are assigned according to eq. 7 of Deason et al. (2011). The Sgr leading tail is clearly seen at  $40^\circ < \Lambda_\odot < 120^\circ$  in both BHBs ( $17 < m - M < 19$ ) and BSs ( $19 < m - M < 21.5$ ). Note also the unambiguous detection of the trailing debris at  $130^\circ < \Lambda_\odot < 190^\circ$ . *Bottom:* Density of the stream stars in the plane of  $\Lambda_\odot$  and the line-of-sight velocity  $V_{\text{SGR}}$ . For this plot, giant stars with  $-9^\circ < B < 9^\circ$  are selected using the criteria in eq. 1 from the SDSS spectroscopic database.

the middle panel of the Figure. Only the stars that lie inside the  $u - g, g - r$  boundary shown in the Left panel of Figure 1 (see Yanny et al. 2000) and within  $-8^\circ < B_\odot < 4^\circ$  are included in this picture. The leading tail can be traced from  $\Lambda_\odot \sim 35^\circ$  to  $\Lambda_\odot \sim 120^\circ$  with both BHB at  $17 < (m - M)_g < 19$  and BS stars at  $(m - M)_g > 19.5$ . The stream signal traced by the A-coloured stars dries up much faster than that traced by the MSTO stars; this is simply the consequence of the declining stream luminosity and the decreasing distance as explained in Niederste-Ostholt et al. (2010).

The trailing tail is expected to enter the SDSS footprint at high  $\Lambda_\odot$ . In the middle panel of Figure 2, there are two density enhance-

ments at  $\Lambda_{\odot} > 150^{\circ}$ : a broad faint cloud at  $16 < (m - M)_g < 17.5$  and a narrow sequence at  $19 < (m - M)_g < 20.5$ . To establish which of the two signals is contributed by the Sgr debris, the 2D histograms of the candidate BHB stars in the corresponding  $(m - M)_g$  ranges are plotted in Figure 3. Dominating the Left panel of Figure 3 are two overdensities each ending sharply at  $|B_{\odot}| > 10^{\circ}$ . The one at lower  $\Lambda_{\odot}$  obviously corresponds to the Sgr leading tail, while the short stubby piece of the stream at higher  $\Lambda_{\odot}$  clearly has not precessed as much as the nearby end of the Branch A (see top panel of Figure 2). The fact that the width of the distribution of the distant BHB stars matches that of the rest of the Sgr stream has already been noted by (Newberg et al. 2003). This picture is distinctly different from the one seen in the Right panel of the Figure, where the shape of the distribution of the brighter BHB-like stars bears little resemblance to the Sgr stream. At around  $\Lambda_{\odot} \sim 110^{\circ}$ , there appears an over-density that could correspond to either the brightest of the leading tail BHBs or stars in the Virgo over-density. Most importantly, at  $\Lambda_{\odot} > 160^{\circ}$ , the stars are distributed in a band perpendicular to the direction of the stream, thus ruling out any connection to Sagittarius.

It is reasonable to conjecture that the debris traced by the distant BHB stars is contributed by the Sgr trailing tail that passed through the Galactic disk and is near its apo-centre at  $\Lambda_{\odot} \sim 170^{\circ}$ . To further test this hypothesis, the line-of-sight (LOS) velocities  $V_{\text{GSR}}$  of all SDSS DR8 giant stars in the vicinity of the equator of the Sgr coordinate system are plotted in the lower panel of Figure 2. The following magnitude, colour, surface gravity and metallicity cuts are applied to pick out the giants:

$$\begin{aligned} 17 < g < 21.5 \\ 0.8 < g - i < 1.6 \\ \log(g) < 3 \\ [\text{Fe}/\text{H}] < 0 \end{aligned} \quad (1)$$

Within  $-9^{\circ} < B_{\odot} < 9^{\circ}$ , the distribution of the stars remaining after the above cuts is dominated by the two narrow sequences. Starting at  $V_{\text{GSR}} \sim 50$  km/s,  $\Lambda_{\odot} \sim 60^{\circ}$  is the Sgr leading tail, with its velocity gently decreasing with longitude down to  $V_{\text{GSR}} \sim -120$  km/s at  $\Lambda_{\odot} \sim 130^{\circ}$ , where it seems to flatten. Wherever the datasets overlap, the leading tail kinematics reported here are in good agreement with the velocities of the M giants reported by Law et al. (2004, 2005). The other similarly narrow overdensity is most prominent at  $\Lambda_{\odot} \sim 180^{\circ}$  where it is at  $V_{\text{GSR}} \sim -50$  km/s. It then increases – somewhat more steeply than the leading tail signal – with diminishing longitude.

Each of the three panels of Figure 2 shows the properties of a different stellar tracer inside the Sgr stream. The underlying logic that links the distribution of MSTO stars on the sky with the distance evolution of the BHBs and the kinematics of the RGB stars is threefold. First, the density enhancements in all three stellar populations are limited to the Sgr orbital plane as represented by the rotated coordinate system of Majewski et al. (2003). Second, both the BHB and the RGB overdensities are narrow enough to match the cross-section of the stream as measured on the celestial sphere. Third, as a function of the longitude  $\Lambda_{\odot}$ , the RGB kinematics evolves in agreement with the distance gradients as traced by the BHB stars. In particular, the LOS velocity of both the leading and the trailing tail goes through zero in the vicinity of the respective apo-centre.

### 2.3 Trailing arm: Connecting the dots

Given the clarity of the stream signal in both distance and the velocity domain, it is straightforward to measure the change in the centroid of the Sgr debris as a function of  $\Lambda_{\odot}$ . To this end, we build the model of the Galactic foreground and the Sgr stream as follows. At each  $\Lambda_{\odot}$ , the latitudinal probability that a star belongs to the stream is Gaussian, while the probability of belonging to the foreground changes linearly with latitude  $B_{\odot}$ . Therefore, there are 4 unknowns describing the centre and the width of the Gaussian and the slope and the normalization of foreground. The sets of 4 model parameters are allowed to evolve freely from bin to bin in longitude  $\Lambda_{\odot}$ . In each bin, the maximum likelihood model is sought using the individual BHB distance modulus values and the RGB velocity values with a brute-force grid search implemented in IDL. As is obvious from the Figure 2, the foreground density field is not exactly linear as a function of  $B_{\odot}$ . Therefore, when fitting the distance modulus signal, only values within  $\pm 1$  mag of the tentative stream centroid were used. Similarly, while modelling the velocity, only the values inside  $\pm 150$  km/s margin were used. The width of the bin in  $\Lambda_{\odot}$  was chosen through trial and error to maintain reasonably high longitudinal resolution while having enough signal-to-noise per bin. The distances are measured in bins that are  $4^{\circ}.7$  ( $6^{\circ}.6$ ) wide, for the leading (trailing) arm respectively. The velocities are measured in bins that are  $6^{\circ}.2$  ( $7^{\circ}.05$ ) wide, for the leading (trailing) arm respectively. The distance and velocity centroids with the associated uncertainties are reported in Tables 1, 2 and 3, 4 respectively and shown in Figure 4.

Top and middle panels of Figure 4 show the distances to the centroids of the BHB stars in the Sgr stream measured as described above. Also shown are the distances measured using the stream's Sub Giant Branch (SGB) stars, as reported by Belokurov et al. (2006). Note, however, that there is an important discrepancy between the SGB and the BHB measurements. The SGB distance moduli  $(m - M)_{\text{SGB}}$  needs to be increased by 0.15 mag to match the values of BHB distances at the same locations. The SGB measurements in Belokurov et al. (2006) are differential with respect to the main body of Sgr dSph and can be placed on the absolute scale only by assuming the overall metallicity of the Stream. Belokurov et al. (2006) suggested that the Stream's stellar population resembles closely that of the remnant and hence assigned the same  $i$ -band magnitude to the SGB in the Stream and the Sgr core. The offset between the SGB and BHB stars measured here implies that the SGB of the Stream is 0.15 magnitudes brighter than the SGB of the remnant and hence more metal poor. This is in good agreement with the recent measurements of metallicity gradients along the Sgr stream (e.g. Bellazzini et al. 2006; Chou et al. 2007; Niederste-Ostholt et al. 2010).<sup>1</sup>

With the accurate distance measurements of the trailing debris covering  $140^{\circ} < \Lambda_{\odot} < 190^{\circ}$  reported here, it is easy to “connect the dots” and conclude that the most natural explanation for the so-called Branch C of Belokurov et al. (2006), confirmed most recently by Correnti et al. (2010) with Red Clump giants, is simply the extension of the trailing tail into the range of lower  $\Lambda_{\odot}$  where it overlaps with the leading tail at  $\Lambda_{\odot} \sim 100^{\circ}$ . The trailing stream lies further out in the halo and follows a steeper distance gradient than predicted by any Sgr disruption model to date. For

<sup>1</sup> Niederste-Ostholt et al. (2010) report a reasonable match between the SGB and the BHB distances along the Sgr stream, however they assume fixed absolute magnitude for BHB stars of  $M_g = 0.7$ , while most of the redder BHB stars have  $M_g \sim 0.5$ .

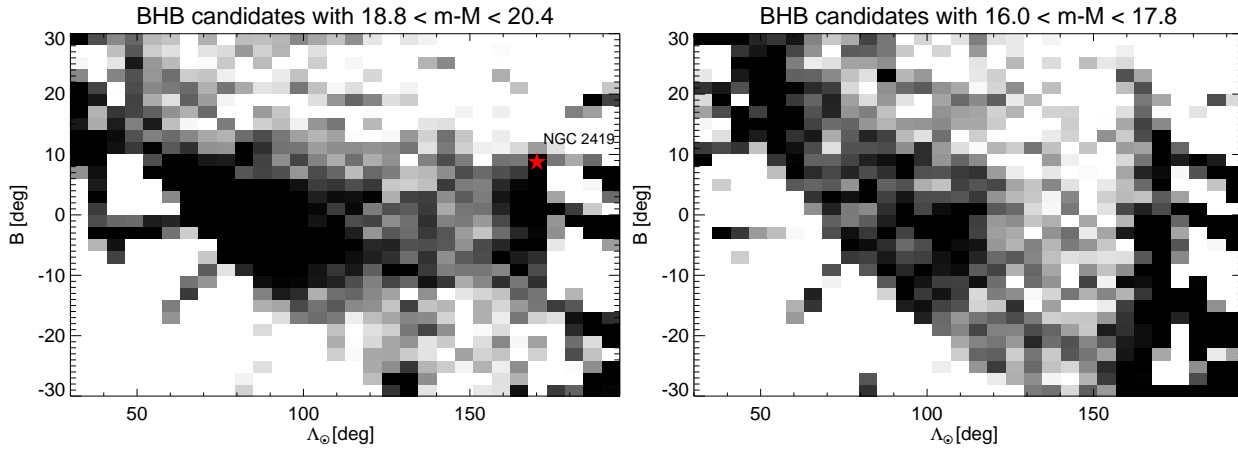


**Figure 3.** Sky density of the BHB candidates. *Left:* Stars with  $18.8 < m - M < 20.4$  (see Middle panel of Figure 2). Both leading tail and trailing tail can be easily discerned. Globular cluster NGC 2419 appears projected right at the edge of the trailing stream. *Right:* Density of the brighter BHB candidate stars. None of the Sgr tails appears distinctly visible in this picture, although an over-density is detected at  $80^\circ < \Lambda_\odot < 120^\circ$ , which could plausibly be attributed either to the portion of the Sgr leading stream falling into this distance range, or to the Virgo Stellar Structure. At high  $\Lambda_\odot$ , a narrow vertical band parallel to the Galactic disk is visible. The A-colored stars in this structure could either be young stars in the disk, alternatively they could be the denizens of the Monoceros stream.

example, in the model of Law & Majewski (2010) the crossing of the leading and trailing tails in the North happens at  $RA \sim 150^\circ$  or  $\Lambda_\odot \sim 140^\circ$ , thus missing it by some  $40^\circ$ . The available kinematics of the trailing tail lend support to our interpretation. The lower panel of Figure 4 shows that as the debris reach the apo-centre at  $\Lambda_\odot \sim 170^\circ$ , the LOS velocity changes sign and goes through zero. The maximum LOS velocity is reached at a point where the line of sight is best aligned with the stream. In the trailing arm velocity data, there is a clear indication of the plateau at  $\Lambda_\odot \sim 135^\circ$ . The LOS velocity is then expected to drop to zero close to the pericentre, which for the trailing tail seems to lie not too far from the point of the crossing with the leading tail.

If the above interpretation is correct, then the Sgr trailing debris are flung out as far as 100 kpc away from the Galactic centre. This in turn implies a difference of  $\sim 50$  kpc between the leading and the trailing apo-centres, which is not predicted by any of the current Sgr disruption models. While the orbital precession is sensitive to the global properties of the potential probed by the orbit, the difference in apo-central distances is also the consequence of the offset in energy and angular momentum of the debris at the moment of stripping, which for systems like Sgr, happens predominantly at pericentre. A larger offset can be either a result of a steeper potential or a larger tidal diameter of the satellite, or indeed, a combination of both.

### 3 NGC 2419

NGC 2419 is rather unusual for a Milky Way globular cluster. Together with  $\omega$ Cen, it deviates from the size-luminosity relation obeyed by other Galactic globulars, as noted, for example, by van den Bergh & Mackey (2004). NGC 2419 appears to have the relaxation time well in excess of Hubble time. In other words, it is much too extended for its stellar mass, which by itself makes it one of the most luminous GCs in the Galaxy. As van den Bergh & Mackey (2004) and others suggest, the NGC 2419's peculiarity could possibly be explained away if it was born in a dwarf satellite of the Milky Way which was then destroyed during accretion leaving the fleshy cluster intact in the gravitational field of the Milky Way's

outer halo. The search is on for the evidence of the past existence of the globular's parent galaxy. van den Bergh & Mackey (2004) predict a spread, albeit possibly quite small, in the metallicities of the cluster's member stars. Most recently, Cohen et al. (2010) seem, at first glance, to have detected exactly that: a small, but measurable spread in the CaT equivalent widths of several tens of the RGB stars in NGC 2419, which could be interpreted as the spread in  $[Fe/H]$  values around the mean of  $-2.1$ . However, in the follow-up high resolution study, Cohen et al. (2011) and Cohen & Kirby (2012) find no detectable spread in  $[Fe/H]$ , but unusually high depletion of Mg and a bizarre anti-correlation between Mg and K. They conclude by stating that no nucleosynthetic source is capable of explaining the chemical makeup of NGC 2419.

Of course, any sign of the tidal debris that can be traced back to the vicinity of NGC 2419 would be a giveaway just as well. Newberg et al. (2003) show that, within the Sgr debris plane, an overdensity of BHBs at distances similar to that of NGC 2419 can be seen in the SDSS photometric data. They therefore speculate that the cluster was once part of the Sgr galaxy. Casetti-Dinescu et al. (2009) on the other hand link the cluster with the Virgo Stellar Stream (which is a part of the Virgo Over-Density) on the basis of the cluster's proximity to the very eccentric orbit predicted from the measured mean radial velocity and the proper motion of the stream. In this paper, we have shown that NGC 2419 does lie close to the plane of the Sgr tidal debris. According to Figure 3, NGC 2419 is situated near the edge of the stream at  $B_\odot \sim 9^\circ$ . Figures 4 and 6 show that NGC 2419 is located right at the apo-centre of the Sgr trailing debris, more than 100 kpc away from the remnant. Finally, the cluster's LOS velocity matches that of the receding trailing debris reaching its apo-centre. If this globular was indeed part of the Sgr dwarf in the distant past, it might not be too surprising that presently it is found further away from both the centroid of the stream and the remnant itself. Had it lived closer to the central parts of Sgr, chances are it would have fallen into the centre of the dwarf galaxy due to the dynamical friction.

There is a slight hint of bimodality in the distribution of the distant BHBs at around  $\Lambda \sim 160^\circ$  in the Left panel of Figure 3. The width of this part of the trailing stream on the sky is  $\sim 20^\circ$ .

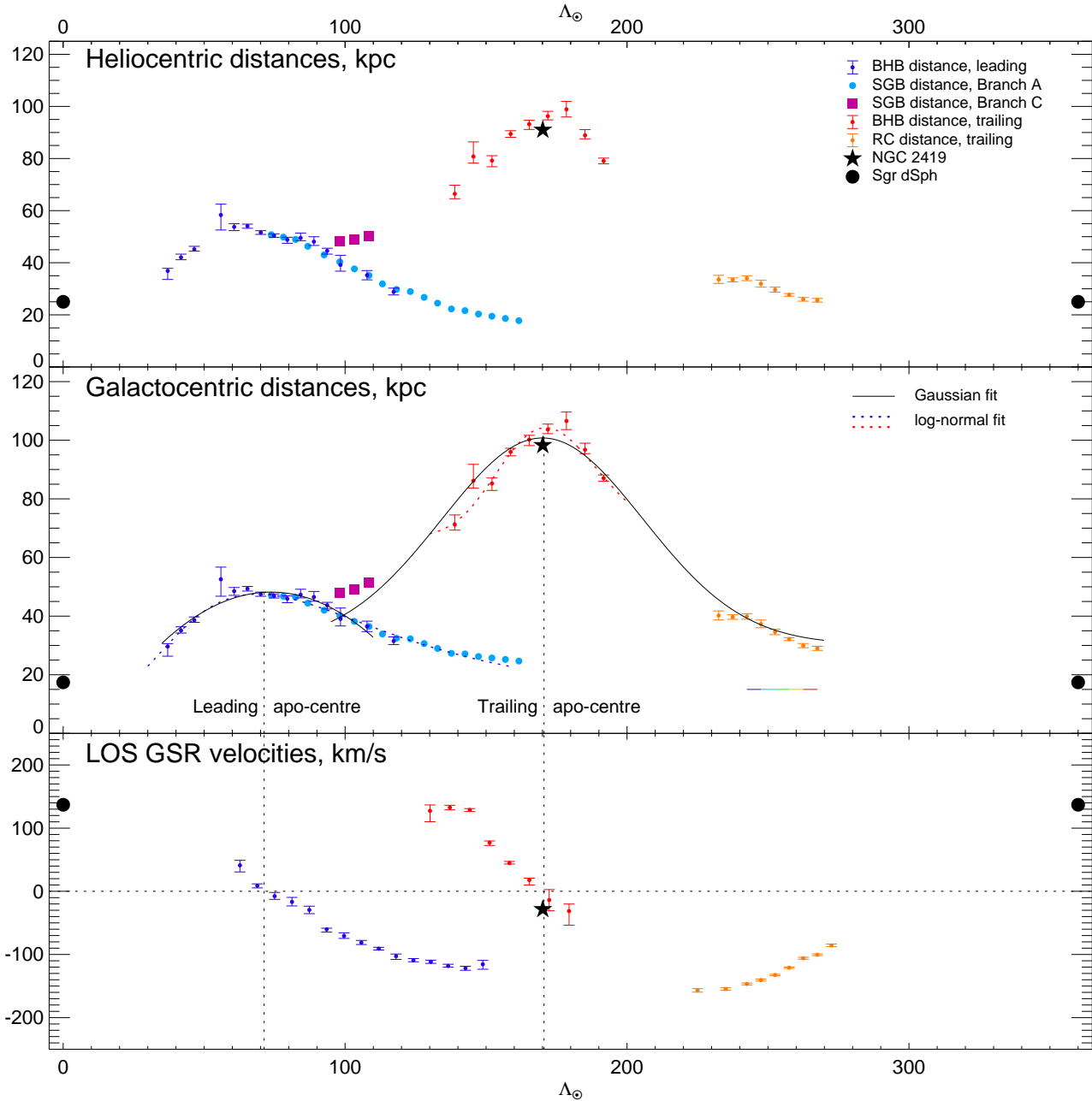


**Figure 4.** Distance and velocity measurements of the Sgr stream. *Top:* Violet (red) data-points with error bars show the centroid of the heliocentric distance of the stream debris at given longitude  $\Lambda_{\odot}$  for the leading (trailing) tail. Blue (magenta) filled circles (squares) are SGB-based Branch A (C) distance measurements from Belokurov et al. (2006) decreased by 0.15 mag to match the BHB signal. Orange data-points with error-bars are RGB-based distance measurements from Koposov et al. (2012) increased by 0.35 mag to correct for the reddening towards the progenitor. A black star marks the location of the globular cluster NGC 2419. *Middle:* Galactocentric stream distances. The stream is assumed to be at  $B = 0^\circ$  everywhere. While this will bias the run of distances for the individual branches of the leading arm at  $\Lambda_{\odot} > 150^\circ$ , this is a very reasonable approximation for the debris around both apo-centres. Violet and red solid curves show the log-normal fits to the data, while black solid curves represent pure Gaussian models. Dotted lines mark the location of the leading and trailing apo-centres. *Bottom:* Measurements of the line-of-sight velocity  $V_{\text{GSR}}$  along the stream. For  $\Lambda_{\odot} < 200^\circ$  the velocity centroids are those based on the SDSS giants stars as presented in Tables 3 and 4, while for  $220^\circ < \Lambda_{\text{odot}} < 280^\circ$  the information is from Koposov et al. (2012). Note that the stream velocity appears to go through zero in the vicinity of the apo-centre.

This is consistent with the detections of the Sgr debris everywhere else on the celestial sphere. However, everywhere else, these  $\sim 20^\circ$  are made up of two distinct components: Branch A and B around the North Galactic Cap (Belokurov et al. 2006), bright and faint trailing stream in the South (Koposov et al. 2012). As judged by the latitude of NGC 2419 in the Sgr coordinate system, it lies much

closer to the debris plane defined by the faint companion to the trailing tail. According to Koposov et al. (2012) this new stream is metal-poor which helps to strengthen its link to NGC 2419 which possesses  $[\text{Fe}/\text{H}] \sim -2.1$

There are examples of globular clusters as extended as NGC 2419 outside the Milky Way. Brodie et al. (2011) discovered a pop-

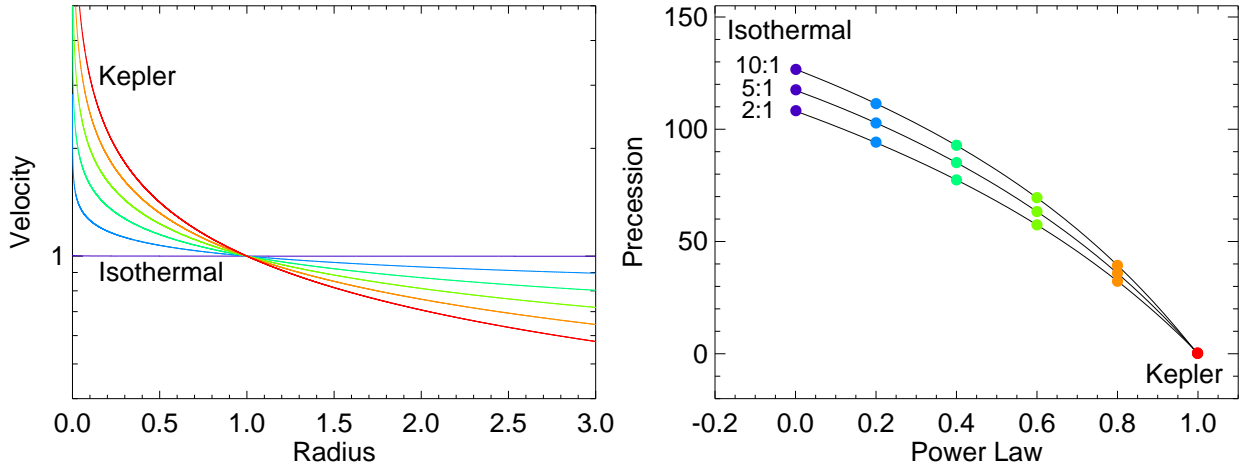


**Figure 5.** *Left:* Circular velocity curves in power-law potentials as a function of radius. *Right:* Apo-centre to apo-centre precession in power-law potentials as a function of the power for three different eccentricities. For each potential (colour-coded according to power-law index), the precession angle in degrees is shown for three orbits with the ratio of apo-centric to peri-centric distance of 10:1, 5:1 and 2:1.

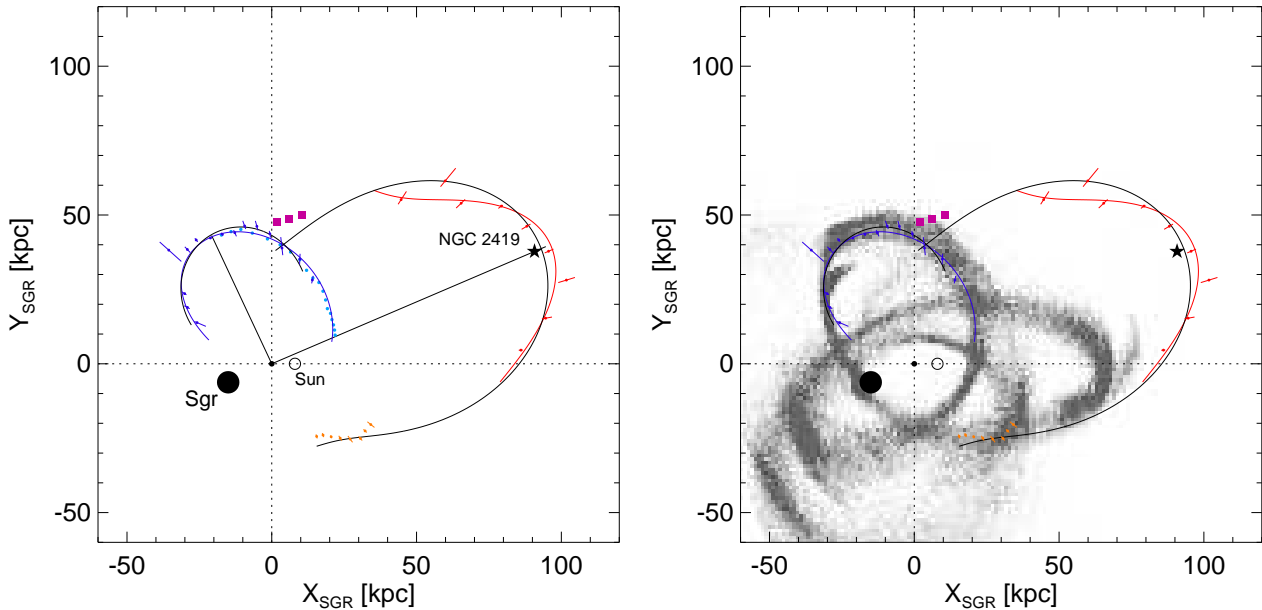


**Figure 6.** Stream precession in the plane of the Sgr orbit. The plane chosen has its pole at Galactocentric  $l_{\text{GC}} = 275^\circ$  and  $b_{\text{GC}} = -14^\circ$ . All symbols, colours and curves are identical to those in Figure 4. *Left:* Note that the actual Galactocentric orbital precession of  $93^\circ$  is slightly lower than the difference between the heliocentric apo-centre phases from Figure 4. *Right:* Comparison with the Sgr disruption model by Law & Majewski (2010) shown as grey-scale density. Note that in the logarithmic halo used in the model, the orbital precession is  $\sim 120^\circ$  and the trailing apo-centre lies in the Galactic disk at  $B_{\text{GC}}^{\text{T}} \sim 0^\circ$  and distance of  $R^{\text{T}} \sim 65$  kpc. This should be contrasted with the new measurement of  $B_{\text{GC}}^{\text{T}} \sim 23^\circ$  and  $R^{\text{T}} = 102.5 \pm 2.5$  kpc.

ulation of low-surface brightness counterparts to Ultra Compact Dwarfs in M87, spanning a similar range in size and luminosity. Huxor et al. (2005) discovered a population of faint ( $M_V \gtrsim -7$ ) and fuzzy globulars with typical sizes  $\sim 30$  pc in the neighboring spiral M31. Interestingly, Mackey et al. (2010) showed that all but one of these extended clusters in Andromeda's outer halo lie - in projection - within the known tidal streams. This points to the dwarf satellites of luminous galaxies as the birth place of extended clusters, at least the ones similar to those discovered by Huxor et al. (2005). Some evidence to support this hypothesis, has been published recently. Da Costa et al. (2009) presented a discov-

ery of an extended globular cluster in a low luminosity dwarf elliptical member of the Virgo group. There are also hints of bimodality in the size distribution of globular clusters in dwarf galaxies in the Local Volume (Georgiev et al. 2009).

With its unusually high (for a Milky Way globular cluster) luminosity of  $M_V = -9.4$ , NGC 2419 may have more in common with so-called Ultra-Compact Dwarf (UCD) galaxies (Drinkwater et al. 2000) than with extended globular clusters. However, not only are the UCDs at least a magnitude more luminous, they also appear to have somewhat inflated velocity dispersions, as evident from the inferred mass-to-light ratios of  $\sim 5 - 10$

similar to that of the nuclei of dwarf ellipticals in clusters of galaxies (e.g. Geha et al. 2002). It is therefore not surprising that one of the more popular UCD formation scenarios involves tidally stripping a dwarf elliptical. As of today, the progenitors of the UCDs have not yet been established with certainty. Also, as Haşegan et al. (2005) show, it is close to impossible to assign an astrophysical class to an object in a certain range of luminosity, size and velocity dispersion as quite a few “dwarf-globular transition objects” exist with properties in between globular clusters and dwarf galaxies. Even though a whole zoo of such transition objects have been uncovered, NGC 2419 is in a class of its own: too luminous but not dense enough for a globular, close to the faint end of UCDs, yet, as has been shown by Baumgardt et al. (2009), it can not boast a mass-to-light ratio out of ordinary.

The genesis of either the faint component of the Sgr stream or NGC 2419 is yet to be established. This paper shows that in 4 out of 6 phase-space coordinates, the stream and the cluster are co-incident. The discovery of Cohen & Kirby (2012) presents a rare opportunity to verify the connection between the two using the unusual abundance pattern in NGC 2419.

## 4 THE PRECESSION OF THE SAGITTARIUS DEBRIS

### 4.1 Orbital precession

The rate with which an orbit precesses in a spherically symmetric gravitational potential depends primarily on how quickly the mass generating the gravity field decays with radius. For example, in Keplerian potentials, the precession angle is  $0^\circ$  to ensure the orbits are closed after one period, while in isothermal haloes, the precession is  $\sim 120^\circ$ . Orbits in the outer regions of spherical galaxies should possess a precession rate somewhere between  $0^\circ$  and  $\sim 120^\circ$ . The precession rate is not solely dependent on the mass decay rate in the host, it is also a weak function of the orbital energy and angular momentum (see equation 3.18 in Binney & Tremaine 2008). The dependence of the orbital precession on the potential and the eccentricity of the orbit is illustrated in Figure 5. The left panel of the Figure shows rotation curves for the family of power law potentials  $\Psi = -\alpha^{-1}r^{-\alpha}$  for various  $\alpha$ . The right panel shows the angle between the successive apo-centre passages in the potential with given  $\alpha$ , for three orbital eccentricities. As can be seen from Figure 5, the precession angle increases as the potential gets flatter. This increase is steeper for more eccentric orbits.

It is not possible to measure the precession of the Sgr progenitor’s orbit directly, but the angle between the leading and the trailing apo-centres encodes the necessary information. The angle between the two apo-centres detected in the SDSS data is calculated as follows. Two simple models are fitted to the Sgr Galactocentric distance data: Gaussian and log-normal. While both completely unphysical, these describe the available data satisfactorily and give an idea of the uncertainty associated with the model mismatch. Overall, the distance to the trailing debris appears to be more Gaussian-like, therefore the Gaussian model is fitted to all the data presented in the top panel of Figure 4. Around the apo-centre, there is a clear asymmetry in the run of the distances, hence the log-normal model is fitted for the range  $130^\circ < \Lambda_\odot < 200^\circ$ . The opposite is true for the leading tail data: the entire tail is modelled as log-normal, while Gaussian is fitted to the distances in the range  $35^\circ < \Lambda_\odot < 110^\circ$ .

For each of the tails, the average of the two model values for the location of the apo-centre is taken.<sup>2</sup>

Solid lines of different colour show the best-fit models for both tails in the middle panel of Figure 4. For the leading tail, the black line is the Gaussian and the blue curve is the log-normal. The leading apo-centre is at  $\Lambda_\odot^L = 71.3 \pm 3.5$ , where it reaches  $R^L = 47.8 \pm 0.5$  kpc. Trailing tail’s apo-centre is at  $\Lambda_\odot^T = 170.5 \pm 1^\circ$  and  $R^T = 102.5 \pm 2.5$  kpc. The red curve shows the log-normal model, while black is the Gaussian. In the heliocentric coordinate system of Majewski et al. (2003), the differential orbital precession between the leading and the trailing apo-centres is  $\delta\Lambda_\odot = 99.3 \pm 3.5$ . Taking into account the Sun’s distance from the center of the Galaxy  $R_0 = 8$  kpc, the Galactocentric  $\delta\Lambda_{GC} = 93.2 \pm 3.5$ .

Figure 6 shows the Sgr stream detections presented in Figure 4 now in the debris plane defined by the pole at  $(l_{GC}, b_{GC}) = (275^\circ, -14^\circ)$ . The right panel of the Figure compares the current data with the model by Law & Majewski (2010) projected onto the same plane. While most of the data, including the entirety of the leading tail detections and the trailing tail data in the range  $220^\circ < \Lambda_\odot < 280^\circ$  is reproduced by the model extremely well, the distant trailing tail measurements in the range  $100^\circ < \Lambda_\odot < 200^\circ$  clearly do not have any counterpart in this simulation. Both the distance to the trailing apo-centre and its position angle are at odds with the observations. At first glance, it seems that the new data require the Galactic halo mass to drop faster with increasing radius than imposed by the logarithmic model used by Law & Majewski (2010). The matter of inferring the Galactic mass constraints from the Sgr debris detections presented here will be addressed thoroughly in a separate publication (Gibbons et al, in prep.)

### 4.2 Orbital plane precession

The previous Subsection assumed implicitly that the leading and the trailing debris, at least up to their respective apo-centres, stay within the same plane, namely the one defined by  $(l_{GC}, b_{GC}) = (275^\circ, -14^\circ)$ . Is this a reasonable assumption? How fast does the plane of the debris precess? Johnston et al. (2005) show that the M giants in the leading and the trailing tail define Galactocentric planes whose poles are  $\sim 10^\circ$  apart. Taking advantage of the dramatic increase in the depth of the SDSS survey compared to 2MASS, as well as the accurate stream distances based on the BHB stars, it is timely to update the study of the evolution of the plane of the Sgr debris.

Most of the new information supplied by the SDSS is in the North, and so it is the leading tail plane evolution we will concentrate on. We start by removing the Galactic foreground contribution from the distribution of the MSTO star counts. This is done in the coordinate system, similar to the one used above, but rotated slightly to ensure that both branches of the leading tail run at constant latitude throughout the range of longitudes seen by the SDSS (see Left panel of Figure 7). Specifically, this is the plane defined by the pole with  $(l, b) = (99.7, 13.7)$ . In each pixel of the longitude  $\Lambda'_\odot$ , the foreground density is fitted with a linear model. Only the pixels outside the range  $-8^\circ < B'_\odot < 10^\circ$  are taken into account

<sup>2</sup> Whenever the distance or the position angle formal error is smaller than the dispersion between the two models, the dispersion is taken as a proxy for the uncertainty

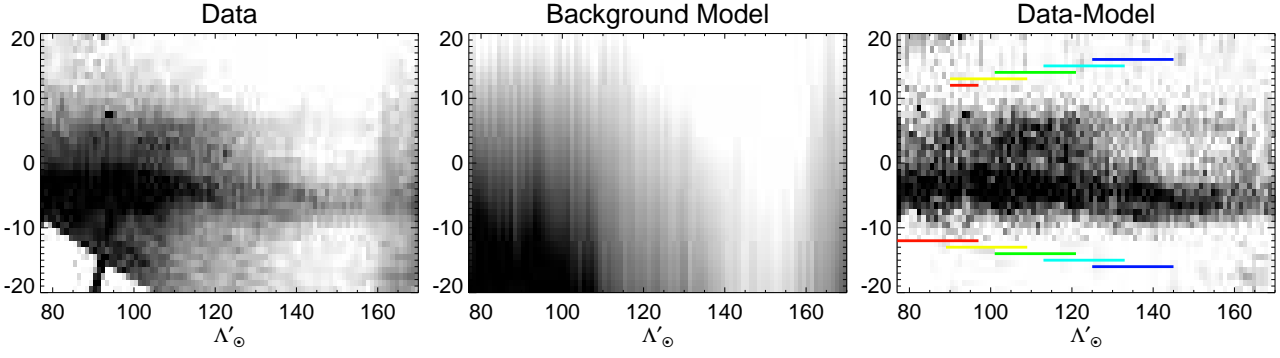


**Figure 7.** Foreground model subtraction for the debris plane analysis. *Left:* Density of the MSTO stars in the coordinate system with the pole at  $l = 99^\circ 7$ ,  $b = 13^\circ 7$  to ensure that both Branch A and B lie at approximately constant latitude. *Middle:* Foreground stellar density modelled as constant slope for each column of the density presented in Left panel. The slope is allowed to vary as a function of the longitude  $\Lambda'_\odot$ . *Right:* Branches A and B revealed after the foreground subtraction. Coloured lines show the sections of the stream used for the debris plane calculation (see Figure 8).

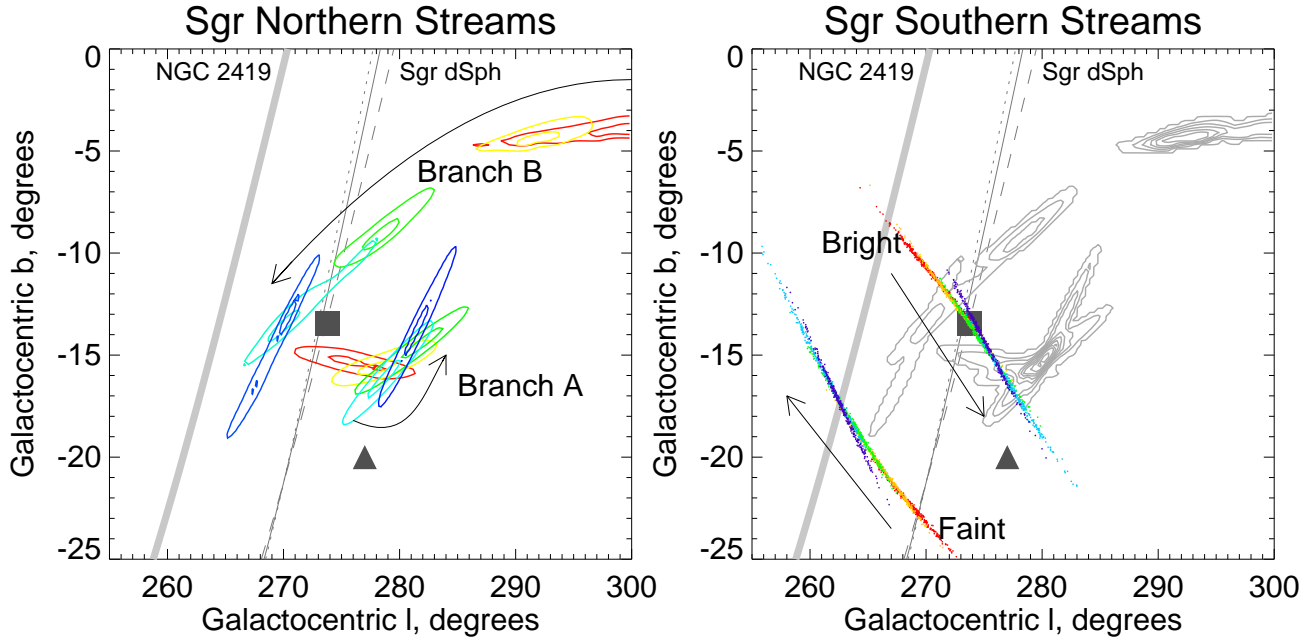


**Figure 8.** Precession of the plane of the Sgr debris in Galactocentric  $l$  and  $b$  coordinates. Three black lines crossing each panel show the great circles drawn by the poles of the planes passing through the current position of the Sgr remnant. Solid is for the Sgr dSph heliocentric distance of 25 kpc, while dotted (dashed) is for the distance increased (reduced) by 5 kpc. Thick light grey line gives the great circle of planes passing through NGC 2419. *Left:* Two sets of contours mark the peaks in the pole density (99.4% and 99.9%) for the five over-lapping sections of the two branches of the leading stream (as indicated in the Right panel of Figure 7). Filled square (triangle) shows the debris plane of the trailing (leading) stream as reported by Johnston et al. (2005). Note the evolution of the leading stream plane away from the trailing pole towards increasing  $l$  and the possible turn-over at  $l_{GC} \sim 280^\circ$  towards decreasing  $b_{GC}$ . The amplitude of the plane precession is markedly different for Branches A and B. Also, note that the two branches have the opposing sense of the plane precession. *Right:* Plane precession for both bright and faint Sgr trailing streams. The Gaussian scatter in distance and  $B$  is added to the stream centroids of pairs of detections reported by Koposov et al. (2012), each coloured point then gives the debris pole determined. There are 300 realisations for each of the 5 pairs of  $\Lambda_\odot$ . The colour changes in the fashion similar to that of the Left panel: from red to dark blue in the direction of the Sgr motion (also see Middle panel of Figure 4 for exact  $\Lambda_\odot$  values). While the precession of the bright trailing debris is consistent with that of the debris in Branch A of the leading tail, the debris in the faint trailing stream component precesses in the direction opposite to its bright counterpart.

**Table 1.** Heliocentric distances to the Sgr Leading stream based on the BHB detections.

$\Lambda_\odot$	37.1	41.8	46.5	55.9	60.6	65.4	70.1	74.8	79.5	84.2	88.9	93.6	98.4	107.8	117.2
$(m - M)_0$	17.83	18.12	18.27	18.83	18.65	18.66	18.56	18.51	18.44	18.47	18.41	18.25	17.96	17.73	17.30
$\sigma_-$	0.20	0.05	0.04	0.23	0.06	0.03	0.03	0.03	0.06	0.05	0.07	0.06	0.14	0.11	0.09
$\sigma_+$	0.06	0.06	0.05	0.15	0.05	0.03	0.03	0.03	0.04	0.08	0.08	0.05	0.20	0.11	0.11

**Table 2.** Heliocentric distances to the Sgr Trailing stream based on the BHB detections.

$\Lambda_{\odot}$	138.9	145.5	152.1	158.7	165.3	171.9	178.5	185.1	191.7
$(m - M)_0$	19.11	19.54	19.49	19.76	19.85	19.92	19.98	19.74	19.49
$\sigma_-$	0.06	0.07	0.07	0.03	0.05	0.03	0.07	0.03	0.03
$\sigma_+$	0.11	0.15	0.05	0.03	0.03	0.04	0.07	0.05	0.03

**Table 3.** Galactocentric velocities of the Sgr Leading stream based on the giant star detections.

$\Lambda_{\odot}$	62.7	68.8	75.0	81.2	87.3	93.5	99.6	105.8	111.9	118.1	124.2	130.4	136.5	142.7	148.8
$V_{\text{GSR}}$	41.1	8.8	-7.6	-16.7	-29.5	-60.2	-70.7	-81.3	-90.8	-102.7	-109.2	-111.6	-118.3	-121.7	-115.5
$\sigma_-$	10.4	3.4	5.1	6.4	5.9	4.4	3.9	2.9	2.1	5.0	2.4	2.4	1.7	3.4	7.9
$\sigma_+$	7.9	3.0	5.8	7.0	6.0	1.8	4.9	3.5	2.2	3.4	2.7	2.6	2.8	2.9	6.1

during the fit. The resulting model foreground is shown in the Middle panel of Figure 7. The residuals of the model subtraction are shown in the Right panel of the Figure. With the foreground (dominated by the Virgo stellar cloud) gone, the leading stream appears with particular clarity.

Each pixel in the right panel of Figure 7 is a line in the space of poles of Galactocentric planes, provided its distance is known. The superposition of such lines defines the cloud of poles corresponding to the group of pixels on the sky. We split Branches A and B into 5 overlapping pieces with the boundaries marked in colour and shown below and above each branch respectively. Left panel of Figure 8 gives the contours of the pole density for each piece of Branch A and B. Pixels belonging to each branch are selected using the simple condition of  $B'_{\odot} < 0$  for Branch A, and  $B'_{\odot} > 0$  for Branch B. The colour-coding used here is identical to the colour-coding in the Right panel of Figure 7. Also plotted here are the two measurements based on the M giants of the trailing and the leading pole reported in Johnston et al. (2005), marked by filled square and triangle respectively. The three lines crossing the figure are the lines of poles of the planes passing through the current position of the remnant. The difference between the lines is the assumed distance to the Sgr dSph.

The earliest it is possible to register the pole of the leading debris is some  $\sim 80^\circ$  away from the remnant. As shown by the red contours, at this stage, the leading debris has already precessed away several degrees from the plane defined by the M giants in the trailing tail. The precession of the leading pole is in the direction of increasing  $l_{\text{GC}}$  and decreasing  $b_{\text{GC}}$ , the same direction as identified by Johnston et al. (2005). As we step along the Branch A, the debris pole first moves further in the same direction, but then turns before reaching the position determined using the M giants. It is unclear whether this turn-around is real as most of the lines in the space of poles contributed by pixels in the segments of the tail at  $\Lambda'_{\odot} > 120^\circ$  are closely aligned as can be gleaned from the shapes of the contours. The signature of the same degeneracy can be seen in the top panels of Figure 3 of Johnston et al. (2005). Nonetheless, we can conclude with certainty that the amplitude of the precession of the plane of the leading debris over  $\sim 100^\circ$  along the stream ought to be less than  $\sim 10^\circ$ .

The evolution of the debris plane defined by the pixels in Branch B is surprisingly different from that of Branch A. The density contours are even more stretched, making it difficult to pinpoint the exact position of the pole for each section of the stream. However, the broad-brush behaviour is apparent: the sense of precession of the Branch B debris pole is opposite to that of Branch A. As one steps along the leading tail away from the remnant in the direction

of Sgr motion, the Branch B pole moves in the direction of *decreasing*  $l$  and *decreasing*  $b$ .

In the South, we do not perform the full debris mapping into the space of the orbital poles, as the SDSS coverage of the stream is limited. Instead, we compute the poles of the planes defined by the pairs of the first 6 detections given in Table 2 of Koposov et al. (2012)<sup>3</sup>. For each such pair, 300 Monte-Carlo trials are carried out to propagate the distance and the latitude  $B_{\odot}$  uncertainty. The resulting debris poles are shown as elongated clouds of dots, whose colour-coding is explained in the Middle panel of Figure 4. The colour changes from red to light blue in the direction of the Sgr motion, similar to the colour-coding scheme used for the leading tail study above. It is reassuring to see that the mean of the five debris pole clouds generated using the bright component of the trailing stream shown in the Figure lies very close to the value of Johnston et al. (2005). Overall, the poles of the debris in the bright trailing stream at  $240^\circ < \Lambda_{\odot} < 280^\circ$  have the same sense of precession as the Branch A debris around  $80^\circ < \Lambda_{\odot} < 100^\circ$ , i.e. the stream angular momentum vector moves in the direction of increasing  $l$  and decreasing  $b$ . Once again, the faint component of trailing stream shows the sense of precession opposite to the bright portion of the tail: the pole moves in the direction of decreasing  $l$  and increasing  $b$ .

Finally, the poles of the debris planes at the positions of the apo-centres seem to lie very close to each other, as judged by the Branch A red contours in the Left panel and dark blue and light blue dots (for the Bright arm) in the Right panel, and reassuringly close to the pole of  $275^\circ, -14^\circ$  chosen for orbit mapping in Section 4.1.

## 5 DISCUSSION AND CONCLUSIONS

We have taken a Swiss Army Knife approach to the SDSS database and mapped the Sgr stellar stream across the sky using three stellar tracers. The MSTO stars helped us define the plane of the Sgr debris, the BHBs provided accurate distances, and the giants gave the clearest view to date of the kinematics of both the leading and the trailing tails as far as 100 kpc in the Galactic halo. Here, is the summary of our main conclusions.

(1) As we push the SDSS data to its limits, that is to the edge of the survey footprint, we are able to discern the apo-centres of the leading and the trailing streams. Distant Sgr debris reported previously

<sup>3</sup> Beyond that, the stream position on the sky is uncertain due to incomplete coverage

**Table 4.** Galactocentric velocities of the Sgr Trailing stream based on the giant star detections.

$\Lambda_{\odot}$	130.1	137.2	144.2	151.2	158.3	165.3	172.4	179.4
$V_{\text{GSR}}$	127.4	132.5	128.8	77.0	44.7	17.8	-13.8	-31.3
$\sigma_{-}$	17.1	3.6	2.5	4.4	1.5	7.9	17.0	22.4
$\sigma_{+}$	9.3	3.6	2.1	2.7	2.5	3.1	16.6	11.2

by Newberg et al. (2003) and Belokurov et al. (2006) link with the new BHB detections to reveal the wide arc of the trailing tail.

(2) Both the orbital precession of the trailing debris and the Galactocentric distances it reaches are at odds with the current state-of-the-art models of Sgr disruption. The angle between the leading and the trailing apo-centres is  $\delta\Lambda_{\text{GC}} = 93^{\circ}2 \pm 3^{\circ}5$ , while their respective distances are  $R^L = 47.8 \pm 0.5$  kpc  $R^T = 102.5 \pm 2.5$  kpc.

(3) We substantiate the detections of the tidal tails and their 3D evolution with the measurements of the debris' line of sight velocity. In particular, we show that around the apo-centres stream's  $V_{\text{GSR}}$  passes through zero.

(4) We show that in 4 out of 6 phase-space coordinates, the peculiar globular cluster NGC 2419 and the Sgr trailing tail coincide. NGC 2419 lies very close to the trailing apo-centre, nearer to the edge of the stream. Given its position and the chemical abundance, it is not impossible that the globular is in fact related to the faint, metal-poor companion of the trailing tail discovered by Koposov et al. (2012).

(5) The plane of the debris delineated by the MSTO stars and anchored with the BHB distances evolves slowly, but noticeably, in the Galactic potential. We also detect a turn-over in the path of the angular momentum of the leading tail.

(6) The sense of precession of the debris plane of both secondary components to the stream, Branch B in the North and the faint trailing tail in the South, appears to be opposite to the main, bright parts of the stream.

Here, we have measured the Galactocentric angle between the apocentres of the leading and trailing tails of the Sgr stream and the difference between their respective distances. The angle through which the orbit turns from one apocentre to the next is largely controlled by the radial profile of the potential. Our measured value is inconsistent with a flat rotation curve, or logarithmic potential, and indicates that the Milky Way's dark matter density falls off more quickly than isothermal. We have also detected the precession of the orbital plane of the Sgr stream. This wallowing, or gentle nutation, of the orbital plane occurs naturally in mildly triaxial potentials, for which evidence exists on other grounds for the Milky Way (e.g., Debattista et al. 2013). In practice, the components of the Sgr progenitor most likely possessed some internal rotation or spin (e.g., Peñarrubia et al. 2010), which can couple to the torques provided by the triaxiality. The complex behaviour of the precession of the plane of the Sgr debris that we have measured is most likely caused by an interplay between the rotational kinematics of the stripped material and the torques exerted by the triaxial gravity field.

Above all, this study has uncovered the stupendous scale of the Sgr stream. The debris stretches over Galactocentric radii from roughly 20 kpc out to at least 100 kpc. This makes the Sgr stream the single most powerful probe of the Milky Way's dark halo. It extends well beyond the gas rotation curve, which gives out at 20

kpc. As the Sgr stream also possesses abundant bright tracers like BHBs, accurate distances and velocities are obtainable almost everywhere. Provided we can decode the message in its runes, it offers momentous constraints on the underlying gravity field at unprecedentedly remote distances. It truly is a touchstone for studies of the very distant dark halo.

## ACKNOWLEDGMENTS

VB acknowledges financial support from the Royal Society (RS) and the European Research Council (ERC). S.K. acknowledges financial support from the STFC and the ERC. MG acknowledges financial support from the RS. EO was partially supported by NSF grant AST0807498.

## REFERENCES

- An, D., et al. 2008, *ApJS*, 179, 326  
 Baumgardt, H., Côté, P., Hilker, M., Rejkuba, M., Mieske, S., Djorgovski, S. G., & Stetson, P. 2009, *MNRAS*, 396, 2051  
 Bellazzini, M., Newberg, H. J., Correnti, M., Ferraro, F. R., & Monaco, L. 2006, *A&A*, 457, L21  
 Belokurov, V. et al. 2006, *ApJ*, 647, L111  
 Belokurov, V., Evans, N. W., Irwin, M. J., et al. 2007, *ApJ*, 658, 337  
 Binney, J., & Tremaine, S. 2008, *Galactic Dynamics: Second Edition*, Princeton University Press, Princeton, NJ USA, 2008.  
 Bovy, J., Allende Prieto, C., Beers, T. C., et al. 2012, *ApJ*, 759, 131  
 Brodie, J. P., Romanowsky, A. J., Strader, J., & Forbes, D. A. 2011, *AJ*, 142, 199  
 Casetti-Dinescu, D. I., Girard, T. M., Majewski, S. R., Vivas, A. K., Wilhelm, R., Carlin, J. L., Beers, T. C., & van Altena, W. F. 2009, *ApJ*, 701, L29  
 Chou, M.-Y., et al. 2007, *ApJ*, 670, 346  
 Cohen, J. G., Kirby, E. N., Simon, J. D., & Geha, M. 2010, *ApJ*, 725, 288  
 Cohen, J. G., Huang, W., & Kirby, E. N. 2011, *ApJ*, 740, 60  
 Cohen, J. G., & Kirby, E. N. 2012, *ApJ*, 760, 86  
 Correnti, M., Bellazzini, M., Ibata, R. A., Ferraro, F. R., & Varghese, A. 2010, *ApJ*, 721, 329  
 Da Costa, G. S., Grebel, E. K., Jerjen, H., Rejkuba, M., & Sharina, M. E. 2009, *AJ*, 137, 4361  
 Deason, A. J., Belokurov, V., & Evans, N. W. 2011, *MNRAS*, 416, 2903  
 Debattista, V. P., Roskar, R., Valluri, M., et al. 2013, *arXiv:1301.2670*  
 Di Criscienzo, M., Greco, C., Ripepi, V., et al. 2011, *AJ*, 141, 81  
 Drinkwater, M. J., Jones, J. B., Gregg, M. D., & Philipps, S. 2000, *PASA*, 17, 227  
 Eyre, A., & Binney, J. 2009, *MNRAS*, 400, 548

- Fellhauer, M., Belokurov, V., Evans, N. W., et al. 2006, *ApJ*, 651, 167
- Fermani, F., & Schönrich, R. 2013, arXiv:1301.1974
- Geha, M., Guhathakurta, P., & van der Marel, R. P. 2002, *AJ*, 124, 3073
- Georgiev, I. Y., Puzia, T. H., Hilker, M., & Goudfrooij, P. 2009, *MNRAS*, 392, 879
- Ghez, A. M., Salim, S., Weinberg, N. N., et al. 2008, *ApJ*, 689, 1044
- Grillmair, C. J., & Dionatos, O. 2006, *ApJ*, 643, L17
- Harris, W. E. 1996, *AJ*, 112, 1487
- Hasegan, M., et al. 2005, *ApJ*, 627, 203
- Helmi, A. 2004, *ApJ*, 610, L97
- Huxor, A. P., Tanvir, N. R., Irwin, M. J., Ibata, R., Collett, J. L., Ferguson, A. M. N., Bridges, T., & Lewis, G. F. 2005, *MNRAS*, 360, 1007
- Ibata, R., Lewis, G. F., Irwin, M., Totten, E., & Quinn, T. 2001, *ApJ*, 551, 294
- Johnston, K. V., Law, D. R., & Majewski, S. R. 2005, *ApJ*, 619, 800
- Koposov, S. E., Rix, H.-W., & Hogg, D. W. 2010, *ApJ*, 712, 260
- Koposov, S. E., Belokurov, V., Evans, N. W., et al. 2012, *ApJ*, 750, 80
- Law, D. R., Majewski, S. R., Skrutskie, M. F., & Johnston, K. V. 2004, ASP Conference Series 327, "Satellites and Tidal Streams", eds Prado F., Martinez-Delgado D., Mahoney T., p. 239
- Law, D. R., Johnston, K. V., & Majewski, S. R. 2005, *ApJ*, 619, 807
- Law, D. R., & Majewski, S. R. 2010, *ApJ*, 714, 229
- Majewski, S. R., Skrutskie, M. F., Weinberg, M. D., & Ostheimer, J. C. 2003, *ApJ*, 599, 1082
- Majewski, S. R., Kunkel, W. E., Law, D. R., et al. 2004, *AJ*, 128, 245
- Mackey, A. D., et al. 2010, *ApJ*, 717, L11
- Niederste-Ostholt, M., Belokurov, V., Evans, N. W., & Peñarrubia, J. 2010, *ApJ*, 712, 516
- Newberg, H. J., Yanny, B., Grebel, E. K., et al. 2003, *ApJ*, 596, L191
- Odenkirchen, M., Grebel, E. K., Dehnen, W., et al. 2003, *AJ*, 126, 2385
- Peñarrubia, J., Belokurov, V., Evans, N. W., et al. 2010, *MNRAS*, 408, L26
- Schlegel, D. J., Finkbeiner, D. P., & Davis, M. 1998, *ApJ*, 500, 525
- Schönrich, R., Binney, J., & Dehnen, W. 2010, *MNRAS*, 403, 1829
- van den Bergh, S., & Mackey, A. D. 2004, *MNRAS*, 354, 713
- Yanny, B., et al. 2000, *ApJ*, 540, 825